

Excited electronic state decomposition of furazan based energetic materials: 3,3'-diamino-4,4'-azoxyfurazan and its model systems, diaminofurazan and furazan

Y. Q. Guo, A. Bhattacharya, and E. R. Bernstein

Citation: *The Journal of Chemical Physics* **128**, 034303 (2008); doi: 10.1063/1.2822283

View online: <http://dx.doi.org/10.1063/1.2822283>

View Table of Contents: <http://aip.scitation.org/toc/jcp/128/3>

Published by the *American Institute of Physics*

COMPLETELY

REDESIGNED!



**PHYSICS
TODAY**

Physics Today Buyer's Guide
Search with a purpose.

Excited electronic state decomposition of furazan based energetic materials: 3,3'-diamino-4,4'-azoxyfurazan and its model systems, diaminofurazan and furazan

Y. Q. Guo, A. Bhattacharya, and E. R. Bernstein^{a)}

Department of Chemistry, Colorado State University, Fort Collins, Colorado 80523-1872, USA

(Received 20 September 2007; accepted 14 November 2007; published online 15 January 2008)

We report the first experimental and theoretical study of gas phase excited electronic state decomposition of a furazan based, high nitrogen content energetic material, 3,3'-diamino-4,4'-azoxyfurazan (DAAF), and its model systems, diaminofurazan (DAF) and furazan ($C_2H_2N_2O$). DAAF has received major attention as an insensitive high energy explosive; however, the mechanism and dynamics of the decomposition of this material are not clear yet. In order to understand the initial decomposition mechanism of DAAF and those of its model systems, nanosecond energy resolved and femtosecond time resolved spectroscopies and complete active space self-consistent field (CASSCF) calculations have been employed to investigate the excited electronic state decomposition of these materials. The NO molecule is observed as an initial decomposition product from DAAF and its model systems at three UV excitation wavelengths (226, 236, and 248 nm) with a pulse duration of 8 ns. Energies of the three excitation wavelengths coincide with the (0-0), (0-1), and (0-2) vibronic bands of the $NO A^2\Sigma^+ \leftarrow X^2\Pi$ electronic transition, respectively. A unique excitation wavelength independent dissociation channel is observed for DAAF, which generates the NO product with a rotationally cold (20 K) and a vibrationally hot (1265 K) distribution. On the contrary, excitation wavelength dependent dissociation channels are observed for the model systems, which generate the NO product with both rotationally cold and hot distributions depending on the excitation wavelengths. Potential energy surface calculations at the CASSCF level of theory illustrates that two conical intersections between the excited and ground electronic states are involved in two different excitation wavelength dependent dissociation channels for the model systems. Femtosecond pump-probe experiments at 226 nm reveal that the NO molecule is still the main observed decomposition product from the materials of interest and that the formation dynamics of the NO product is faster than 180 fs. Two additional fragments are observed from furazan with mass of 40 amu (C_2H_2N) and 28 amu (CH_2N) employing femtosecond laser ionization. This observation suggests a five-membered heterocyclic furazan ring opening mechanism with rupture of a CN and a NO bond, yielding NO as a major decomposition product. NH_2 is not observed as a secondary decomposition product of DAAF and DAF. © 2008 American Institute of Physics. [DOI: 10.1063/1.2822283]

I. INTRODUCTION

Energetic materials, defined as controllable storage systems of chemical energy, have numerous military and industry applications as propellants, fuels, explosives, and pyrotechnics. Recently a series of furazan based new energetic materials, especially 3,3'-diamino-4,4'-azoxyfurazan (DAAF), has received great attention due to their favorable properties including good heat resistivity, high heat of formation, low sensitivity, and good detonation performance for applications as high explosives, fuels, and propellants.¹ The structure of DAAF (illustrated in Fig. 1) consists of two aromatic amino furazan rings connected by an azoxy group. As an excellent candidate for an insensitive energetic material, DAAF has acceptable thermal stability and compatibility for solid propellant applications and can be used as an energetic additive to modify the blast properties of nitramine based

composite propellant formulations. In addition, DAAF is also an attractive additive for rocket propellant and triamino trinitrobenzene based explosive formulations. Several studies of the relative thermal stability and detonation performance of DAAF in condensed phase have been performed.²⁻⁴ Differential scanning calorimetry (DSC) and thermogravimetric (TG) analysis of the thermal decomposition of DAAF reveal that it is stable up to 230 °C and that NH_2OH , NH_2CN , NH_3 , and HCN are major thermal decomposition products of DAAF.⁵ Based on the decomposition product distribution, a possible pathway for thermal decomposition of DAAF in the condensed phase has been suggested to be simultaneous cleavage of furazan rings and the azoxy group.

Diaminofurazan (DAF) (see Fig. 1), one of the nonenergetic model systems for furazan based energetic materials, is used as a precursor in the synthesis of many furazan based, high nitrogen content, insensitive energetic materials, including DAAF. Although DAF does not have the promising energetic features of DAAF, it displays great potential as

^{a)}Electronic mail: erb@lamar.colostate.edu.

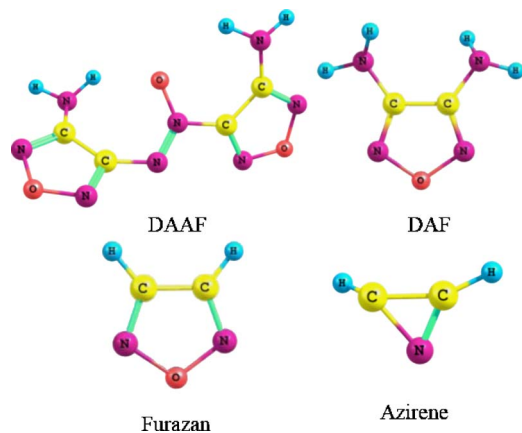


FIG. 1. (Color online) Chemical structures of a furazan based energetic material (DAAF) and its model systems (DAF and furazan) and an intermediate azirene.

ballistic modifier in 1,3,5-trinitro-1,3,5-triazacyclohexane (RDX) incorporated, double base propellant formulations. DSC and differential thermal analysis reveal that DAF thermally decomposes in condensed phase through a two stage pathway in which kinetics of the initial stage of thermal decomposition of DAF is governed by an activation energy of 67 kJ/mol. Gaseous species, such as CN, NH, OH, and oxides of nitrogen, have been identified as thermal decomposition products of DAF through TG-Fourier transform infrared analysis.⁶ The suggested mechanism for the initial thermal decomposition of DAF in condensed phase is rupture of the C–NO bond. For the furazan molecule, which forms the backbone of DAAF and DAF, both gas phase thermal decomposition and photolysis in ether solution reveal that the cleavage of two ring-bonds (C–C and N–O) followed by subsequent rearrangement of the ring yields hydrogen cyanide (HCN) and hydrogen isocyanate (HNCO) as products.^{7,8}

Although the aforementioned studies of thermal decomposition of DAAF and DAF in condensed phase have exposed the thermal stability and thermal decomposition mechanisms for these materials, little information about the difference between intramolecular and intermolecular behaviors, as well as the fundamental decomposition properties of the individual molecules, can be extracted. Additionally, ignition processes involving sparks, shock, slow/rapid heating, lasers, and arcs can all initiate the decomposition reaction of energetic material by generating excited electronic states. Decomposition of energetic materials from excited electronic states has been experimentally proved to play an important role in their overall decomposition mechanisms and kinetics.^{9–14} Thus, investigations of isolated, gas phase molecular decomposition of DAAF and its model systems (DAF and furazan) in excited electronic states will yield an improved understanding of the initial excited electronic state decomposition mechanisms and dynamics of furazan based energetic materials at a fundamental level. To the best of our knowledge, no investigation of the gas phase unimolecular decomposition of furazan based energetic materials and model systems has been reported in literature to date.

This present work reports the first systematic experimental and theoretical study of the excited electronic state de-

composition of these materials. DAF and furazan are selected as model systems because DAAF and these two molecules have similar delocalized aromatic five-membered heterocyclic rings that have spectroscopically active low lying (π, π^*) excited electronic states. On the other hand, DAF and furazan are nonenergetic materials. Therefore, a systematic comparison of the excited electronic state decomposition mechanism for DAAF and its model systems (DAF and furazan) will generate more insight into and understanding of the initial decomposition mechanisms and dynamics of furazan based energetic materials.

Both nanosecond energy resolved and femtosecond time resolved spectroscopies have been employed to investigate the excited electronic state decomposition mechanisms and dynamics of isolated gas phase furazan based molecules (DAAF, DAF, furazan). These three molecules are excited to their (π, π^*) excited electronic state by absorption of a single UV photon and a dissociation product, nitric oxide (NO) is observed by a one-color (1+1) resonance enhanced two-photon ionization (R2PI) scheme using time of flight mass spectrometry (TOFMS) detection. Three vibronic transitions [$A^2\Sigma^+(v'=0) \leftarrow X^2\Pi(v''=0,1,2)$] of the NO molecule from both DAAF and DAF are observed; only two vibronic bands of the NO product from furazan are observed. The NO product from DAAF is generated through an excitation wavelength independent nonadiabatic dissociation channel and characterized by a rotationally cold (20 K) and a vibrationally hot (1260 K) internal energy distribution. The rotational and vibrational distributions of the NO product from DAF and furazan are dependent on the excitation wavelengths. Complete active space self-consistent field (CASSCF) calculations are pursued on furazan and DAF to generate more detailed energetics of their excited electronic state decomposition pathways. These calculations reveal that an energy barrier for the conical intersection between an (n, π^*) excited electronic state and ground electronic state plays an important role in the excited electronic state decomposition pathways of DAF and furazan. CASSCF calculations on DAF and furazan suggest a five-membered heterocyclic furazan ring opening mechanism with rupture of CN and NO bonds yielding NO as a major decomposition product from their (π, π^*) excited electronic state. Femtosecond pump-probe experiments at 226 nm show that the formation dynamics of the NO product from DAAF falls into the time scale of our laser pulse duration (180 fs). Two additional fragments with mass of 40 amu ($C_2H_2N^+$) and 28 amu (CH_2N^+) are observed in the mass spectrum of furazan for 226 nm (1+1) femtosecond ionization. NH_2 is not observed as a secondary decomposition product of DAAF and DAF.

II. EXPERIMENTAL PROCEDURES

Detailed experimental procedures for both nanosecond mass resolved excitation spectroscopy and femtosecond laser pump-probe spectroscopy have been described in our previous publications.^{15–18} Briefly, the experimental setup consists of laser systems with both nanosecond and femtosecond time duration pulses (10 Hz), a supersonic jet expansion nozzle with a laser desorption attachment, and two vacuum cham-

bers [a time of flight mass spectrometer chamber and a laser induced fluorescence (LIF) chamber]. For the nanosecond laser experiments, a single pump-probe laser beam at three wavelengths (226, 236, and 248 nm) is used both to initiate dissociation of furazan based molecules and to detect NO following a one-color (1+1) R2PI scheme [$A^2\Sigma^+(v'=0) \leftarrow X^2\Pi(v''=0,1,2)$ and $I \leftarrow A$ transitions] through TOFMS. The three UV laser wavelengths used in the nanosecond laser experiments are generated by a pulsed dye laser, pumped by the second harmonic (532 nm) of a neodymium doped yttrium aluminum garnet laser's fundamental output (1.064 μm), in conjunction with a nonlinear wavelength extension system. The typical pulse energy of the UV laser is 200–600 $\mu\text{J}/\text{pulse}$ depending on the exact wavelength of interest for a one-color experiment, which gives a laser beam intensity (I) $\sim (1.3\text{--}4) \times 10^7 \text{ W}/\text{cm}^2$ for an 8 ns pulse duration at a focused beam diameter of 0.5 mm. For detection of a NH_2 product from DAF and DAAF through TOFMS, an UV laser beam at 226 nm is used to initiate the dissociation of the parent molecules and two additional laser beams are required to excite and ionize the NH_2 product: one at 600 nm and another at 118 nm corresponding to $A^2A_1(0,9,0) \leftarrow X^2B_1(0,0,0)$ and $I \leftarrow A$ transitions, respectively. For the detection of the NH_2 product through LIF, only one additional laser beam (569 nm) is required to excite the NH_2 $A^2A_1(0,10,0) \leftarrow X^2B_1(0,0,0)$ transition. Detection of the NH_2 product from DAF and DAAF has been calibrated by the observation of the NH_2 radical generated by photolysis of ammonia (NH_3) at 193 nm inside a quartz capillary attached to the pulse nozzle.

For femtosecond pump-probe experiments, a single laser beam at 226 nm is equally split into pump and probe beams. The sample molecules are excited by the pump beam and dissociate according to their dissociation dynamics. The dissociation products are subsequently ionized by the delayed probe beam and detected via TOFMS. By delaying the probe beam with respect to the pump beam, product appearance times can be determined. The femtosecond laser light is generated by a femtosecond laser system consisting of a self-mode-locked Ti:sapphire oscillator (KM Labs), a homemade ring cavity Ti:sapphire amplifier, and a commercial traveling optical parametric amplifier of superfluorescence (Light Conversion) system. Pulse duration of the deep UV laser pulse is measured to be 180 fs using a self-diffraction autocorrelator and off-resonance two-photon absorption of the furan molecule.¹⁹ Typical pulse energy of the deep UV output is $\sim 1 \mu\text{J}/\text{pulse}$. For one-color time resolved investigations, the energy of the pump and probe pulses are kept at an optimum value of $\sim 200 \text{ nJ}/\text{pulse}$ ($I \sim 5.66 \times 10^8 \text{ W}/\text{cm}^2$) to improve signal-to-noise ratio and to avoid uncontrolled fragmentation due to multiphoton absorption by the parent molecule.

The isolated gas phase DAAF and DAF molecules are produced through a combination of matrix assisted laser desorption and supersonic jet expansion. The nozzle employed for the sample beam generation is constructed from a Jordan Co. pulsed valve and a laser desorption attachment.^{20,21} Sample drums for matrix desorption are prepared by wrapping a piece of porous filter paper around a clean aluminum

drum. A solution of equimolar amounts of sample and matrix (R6G dye) in acetone is uniformly sprayed on the sample drum. An air atomizing spray nozzle (Spraying System Co.) with siphon pressure of 10 psi g (gauge) is used to deposit the DAAF/DAF and R6G on the drum surface. During the spraying, the drum is rotated and heated with a halogen lamp to make sure that the coating is homogeneous and dry. The dried sample drum is then placed in the laser ablation head/nozzle assembly and put into a vacuum chamber. In order to maintain a fresh sample area for each laser ablation shot, a single motor is used to rotate and translate the sample drum simultaneously. DAAF/DAF molecules are desorbed from the drum by laser ablation at 532 nm, entrained in the flow of helium carrier gas through a $2 \times 60 \text{ mm}^2$ channel in the ablation head, and expanded into the vacuum chamber.^{22,23} Since furazan is liquid with a high vapor pressure (170 Torr at 25 °C), a 1% furazan-He gas mixture is prepared by pre-mixing He carrier gas with the vapor of a liquid furazan sample and directly expanded into the vacuum system to form a molecular beam.

The experiment is run at a repetition rate of 10 Hz. The timing sequence for the pulsed nozzle, ablation laser, and ionization laser is controlled by a time delay generator (SRS DG535). The molecular beam is perpendicularly crossed by an UV laser beam that is focused to a spot size of about 0.5 mm at the ionization region of a time of flight mass spectrometer. A background pressure of 1×10^{-5} Torr is maintained in the vacuum chamber during the experiment. Ion signals are detected by a microchannel plate detector. Signals are recorded and processed on a personal computer using a boxcar averager (SRS SR 250) and an analog-to-digital conversion card (Analog Devices RTI-800). For time resolved experiments, the delay time between the pump and probe beams is controlled by a microtranslation stage (Thorlabs, LNR50SEK1) with a step size of 13 fs. Each point on the pump-probe transient spectrum corresponds to an average intensity resulting from 100 laser shots. Commercial furazan and DAF (Labotest) are used without any additional purification. DAAF is supplied by Los Alamos National Laboratory (Hiskey) and is used without any further purification.

III. COMPUTATIONAL PROCEDURES

Potential energy surface calculations and geometry optimizations for furazan and DAF are executed at the CASSCF/6-31G* level of theory with GAUSSIAN03 program.²⁴ No symmetry restrictions are applied during the calculations. For the excited state potential energy surface calculations, the minimum active space comprises 10 electrons in 7 orbitals, denoted as CASSCF(10,7), for furazan and 14 electrons in 9 orbitals, denoted as CASSCF(14,9), for DAF. Orbitals used in the active space are three bonding π , two antibonding π^* , and two in-plane N nonbonding $n\sigma_{\text{N}}$ for furazan. In addition to these orbitals, two more nonbonding $n\pi_{\text{N}}$ of the amino groups of DAF, which can take part in the π delocalization of the ring, are included in the active space of DAF. The active orbitals are shown in Fig. 2. The 2s nonbonding orbital of the O atom is excluded from the active

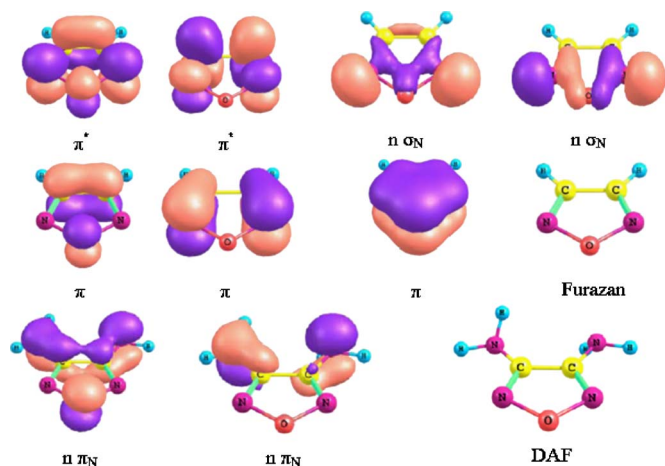


FIG. 2. (Color online) Orbitals used in the active space of CASSCF calculations for furazan and DAF. Three bonding π orbitals, two antibonding π^* orbitals, and two in-plane N nonbonding $n\sigma_N$ orbitals are included in the active space for furazan. In addition, two more nonbonding $n\pi_N$ of the amino groups of DAF are included in the active space for DAF.

space because it is lower in energy than the above orbitals and does not take part in the excitation. Vertical excitation energies are computed by state averaging over the ground state (S_0) and two successive singlet excited states (S_1 and S_2) with equal weights. For reliable estimation of vertical excitation energies, MP2 correlated CASSCF energies are also calculated with the active spaces (10,7) and (14,9) for furazan and DAF, respectively. As the S_1 excited electronic surface for both furazan and DAF is an (n, π^*) excited state, the active space for the optimization of the critical points (local minimum and conical intersections) on the S_1 surface should include all the bonding and antibonding π orbitals and two in-plane N nonbonding $n\sigma_N$ orbitals. The geometries of the critical points are optimized with state averaging over S_0 and S_1 states with equal weights. Thus, the S_1 minimum denoted as $(n, \pi^*)_{\min}$ and two conical intersections, one between the S_1 and S_0 ground electronic surfaces, denoted as $(S_1/S_0)_{CI}$ and another between the S_2 and S_1 excited electronic surfaces, denoted as $(S_2/S_1)_{CI}$ are optimized with active spaces (10,7) and (14,9) for furazan and DAF, respectively. On the other hand, as the S_2 excited electronic surface is a (π, π^*) excited state, critical points [local minimum, denoted as $(\pi, \pi^*)_{\min}$, and conical intersection between S_2 surface and the S_0 ground electronic surface denoted as $(S_2/S_0)_{CI}$] are first optimized with reduced active spaces (6,5) and (10,7) for furazan and DAF, respectively, including only π bonding and antibonding orbitals into their active space. Then single point energies are calculated for these critical points on the S_2 surface to obtain relative energy differences with large active spaces (10,7) and (14,9) for furazan and DAF, respectively. Transition state (TS) structures on the S_0 ground electronic surface are characterized by analytical frequency calculations. The geometry of DAAF shown in Fig. 1 is only optimized at the MP2/6-311G^{**} level of theory.

IV. EXPERIMENTAL RESULTS

A detection scheme diagram for the investigation of the excited electronic state decomposition of furazan based en-

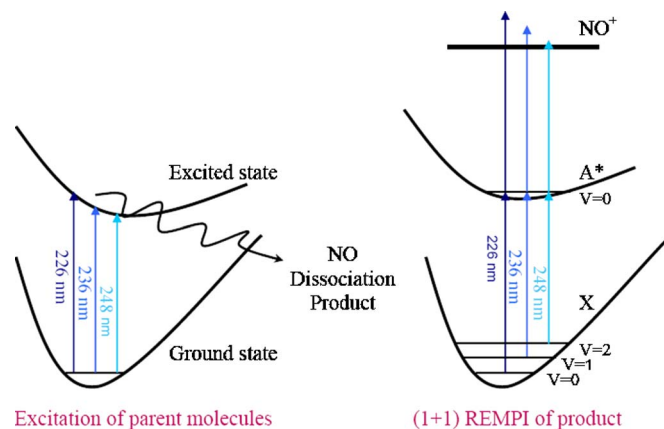


FIG. 3. (Color online) Excitation processes and detection schemes to elucidate the excited electronic state decomposition of furazan based molecules. The parent molecule is excited and fragmented by absorption of single UV photon at three excitation wavelengths, and the product (NO molecule) is probed through one-color (1+1) R2PI technique. Energies of the three excitation wavelengths coincide with three vibronic transitions [$A^2\Sigma^+ \leftarrow X^2\Pi(v''=0, 1, 2)$] of the NO molecule.

ergetic materials and the model systems is shown in Fig. 3. The parent molecule of interest is excited to an excited electronic state by absorption of a single UV photon of one of the three excitation wavelengths (226, 236, and 248 nm). The parent molecules decompose into products through certain decomposition pathways. In nanosecond laser experiments, nitric oxide (NO) is observed as a major initial dissociation product in the excited electronic state decomposition of DAAF, DAF and furazan. The NO product is probed using a one-color (1+1) R2PI detection scheme through TOFMS. The three excitation wavelengths used in this work also correspond to the resonance absorption of (0-0), (0-1), and (0-2) vibronic bands of the $A^2\Sigma^+ \leftarrow X^2\Pi$ electronic transitions of the NO product, respectively. By scanning the nanosecond laser excitation wavelength, a (1+1) R2PI rotationally resolved spectrum of the NO product from different parent molecules is recorded.

(1+1) R2PI spectra of the three vibronic transitions, $A^2\Sigma^+(v'=0) \leftarrow X^2\Pi(v''=0, 1, 2)$, of the NO molecule observed from decomposition of DAAF from its excited electronic state are shown in Fig. 4. The three spectra in this figure have similar rotational structure but have a different absolute intensity for each vibronic band. The most intense feature in each spectrum of NO from DAAF can be assigned as the $(Q_{11}+P_{12})$ band head of each vibronic band, and the less intense features within each spectrum are due to other rovibronic transitions.^{25,26} Spectral simulation based on the Boltzmann population distributions for the three vibronic transitions of the NO product from DAAF produces similar rotational temperatures (~ 20 K) for the three vibrational levels ($v''=0, 1, 2$) in the ground electronic state. The vibrational temperature of the NO product from DAAF can also be obtained by simulating the relative intensities among the observed vibronic bands using Boltzmann population distribution analysis. By comparing the experimental data with simulation at different vibrational temperatures, the vibrational temperature of the NO product from DAAF is estimated to be 1260 K.

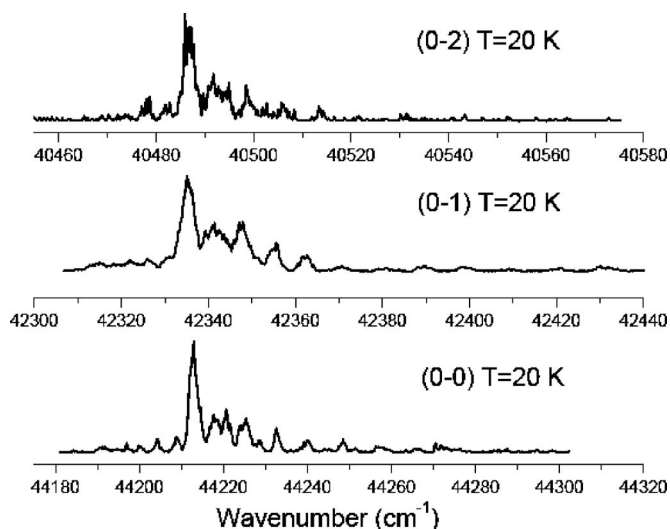


FIG. 4. One-color (1+1) R2PI spectra of the vibronic transitions [$A^2\Sigma^+(v'=0) \leftarrow X^2\Pi(v''=0, 1, 2)$] of the NO product from the excited electronic state decomposition of DAAF molecule. Rotational temperature simulations with Boltzmann distribution show that the three observed vibrational levels on the ground electronic states have a similar rotational temperature of 20 K.

Although the matrix assisted laser desorption technique is a good method to place easily fragmented, fragile molecules in the gas phase without fragmentation, great efforts are taken in our previous and present works to ensure that the sample molecules are not fragmented in the ablation process.^{15–18} Three different methods have been employed to explore this issue: comparison of NO velocity distributions from the nozzle, determination of arrival time for the NO signal intensity as a function of nozzle/pump laser timing, and NO rotational and vibrational temperature determinations as a function of source of NO. These methods demonstrate that NO from DAAF is generated at the ionization region of the TOFMS, not in the laser desorption region of the nozzle.

Similar (1+1) R2PI spectra of three vibronic transitions, $A^2\Sigma^+(v'=0) \leftarrow X^2\Pi(v''=0, 1, 2)$, of the NO molecule obtained from the excited electronic state decomposition of DAF are shown in Fig. 5. The (0–0) and (0–1) vibronic bands of the NO product from DAF show similar rotational patterns to those of the NO product from DAAF, and the rotational temperature of these two bands is also about 20 K. The (0–2) vibronic band of the NO product from DAF shows much hotter rotational distribution than that of the (0–0) and (0–1) vibronic bands. Spectral simulation to the (0–2) band yields a rotational temperature of about 100 K. The excited electronic state decomposition of the furazan molecule generates NO products with only $v''=0$ and 1 populations, and the spectra of the two observed vibronic bands, (0–0) and (0–1), of the NO product are illustrated in Fig. 6. The spectral structure of the (0–0) band of the NO product from furazan is similar to that of the NO product from both DAAF and DAF; however, the (0–1) vibronic band shows a hot rotational pattern with a temperature of about 130 K. No (0–3) spectrum of NO from DAF and (0–2) spectrum of NO from furazan are obtained.

Only NO product is observed in nanosecond laser ex-

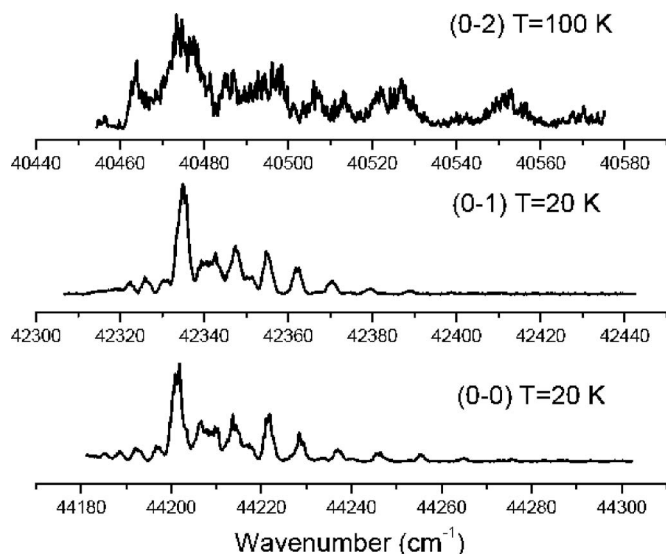


FIG. 5. One-color (1+1) R2PI spectra of the vibronic transitions [$A^2\Sigma^+(v'=0) \leftarrow X^2\Pi(v''=0, 1, 2)$] of the NO product from the excited electronic state decomposition of DAF molecule. Rotational temperature simulations with Boltzmann distribution show that the $v''=0$ and 1 vibrational levels on the ground electronic state have a similar rotational temperature of 20 K, and the $v''=2$ vibrational level has a rotational temperature of 100 K.

periments as the major initial product in the excited electronic state decomposition of DAAF, DAF and furazan. Table I gives rotational temperatures for each populated vibrational level of the NO product from both the energetic material and its and model systems. The NO product from DAAF displays similar cold rotational distributions (20 K) at all three excitation wavelengths (226, 236, and 248 nm). This implies that the excited electronic state decomposition of DAAF follows a single, excitation wavelength independent dissociation channel. The model systems, on the other hand, show excitation wavelength dependent dissociation

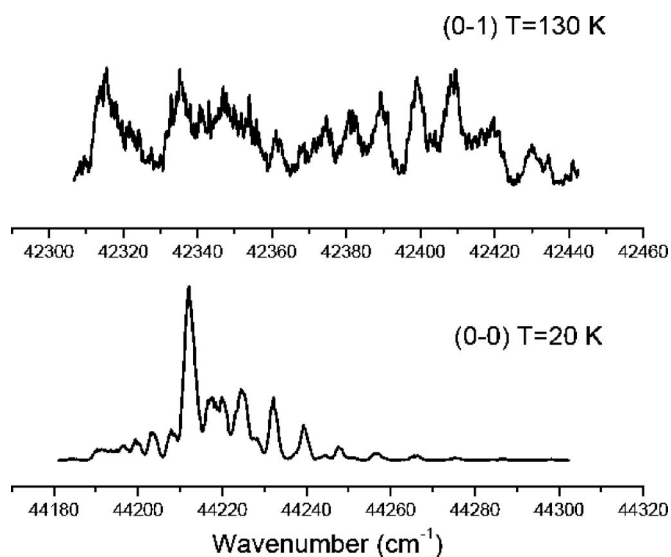


FIG. 6. One-color (1+1) R2PI spectra of the vibronic transitions [$A^2\Sigma^+(v'=0) \leftarrow X^2\Pi(v''=0, 1)$] of the NO product from the excited electronic state decomposition of furazan molecule. Rotational temperature simulations with Boltzmann distribution show that the $v''=0$ vibrational level on the ground electronic states have a rotational temperature of 20 K, and the $v''=1$ vibrational level has a rotational temperature of 130 K.

TABLE I. Rotational temperatures for the $[A^2\Sigma^+(v'=0) \leftarrow X^2\Pi(v''=0, 1, 2)]$ transitions of the NO product from nanosecond laser excited electronic state decomposition of energetic material DAAF and its model systems furazan and DAF.

Compounds	Rotational Temp.	Rotational Temp.	Rotational Temp.
	$A \leftarrow X (0-0)$ (K)	$A \leftarrow X (0-1)$ (K)	$A \leftarrow X (0-2)$ (K)
DAAF	20	20	20
Furazan	20	130	
DAF	20	20	100

channels. For example, dissociation of furazan at 236 nm and that of DAF at 248 nm render hot rotational distributions for the NO product, whereas excitation of furazan at 226 nm and that of DAF at 226 and 236 nm yield cold rotational distributions for the NO fragmentation product. This difference in mechanistic behavior can be rationalized by the fact that DAAF must have dissociative excited states which can provide a barrierless single decay channel for excited state decomposition of this material. For the model systems, on the other hand, there is some barrier in the excited state decomposition pathway which can alter the decomposition channel from the excited electronic state. More detailed exploration of these different evolution pathways from the excited electronic state with respect to relevant reaction coordinates will be presented in Sec. VI.

The NH_2 radical generated by photolysis of NH_3 at 193 nm excitation is detected by both TOFMS and LIF. These detection schemes and rotationally resolved two-color $(1+1')$ R2PI spectrum of NH_2 obtained from photolysis of NH_3 serve as standard calibration of the apparatus for the detection of the NH_2 product from DAF and DAAF. No NH_2 product is observed by either TOFMS or LIF detection from decomposition of DAF or DAAF, which eliminates the possibility of the NH_2 as a secondary decomposition product (or intermediate precursor) for the excited electronic state decomposition of these two molecules.

The time of flight mass spectra of DAAF, DAF, and furazan obtained by the resonance excitation with 180 fs laser pulses at 226 nm are shown in Fig. 7. The NO molecule corresponding to mass channel of 30 amu is still the only observed decomposition product from both DAAF and DAF in the femtosecond time regime. No parent ion is observed for any of these three molecules. For the furazan molecule, besides the NO mass channel, two additional mass channels corresponding to 40 and 28 amu are observed. These two mass channels can be assigned as azirinylium cation ($\text{C}_2\text{H}_2\text{N}^+$) and methylene amidogenyl cation (H_2CN^+), respectively. The azirinylium cation consists of three-membered ring with aromatic properties (shown in Fig. 1) and is the most stable species among the possible $\text{C}_2\text{H}_2\text{N}^+$ isomers.²⁷ Methylene amidogenyl cation has also been observed from two-color nanosecond pump-probe experiment of the excited electronic state decomposition of furazan at 226 nm (pump) excitation and products are probed by 193 nm. According to the fragments observed due to the excited electronic state decomposition of furazan, both in the nanosecond and the femtosecond time regimes, a five-membered heterocyclic furazan ring

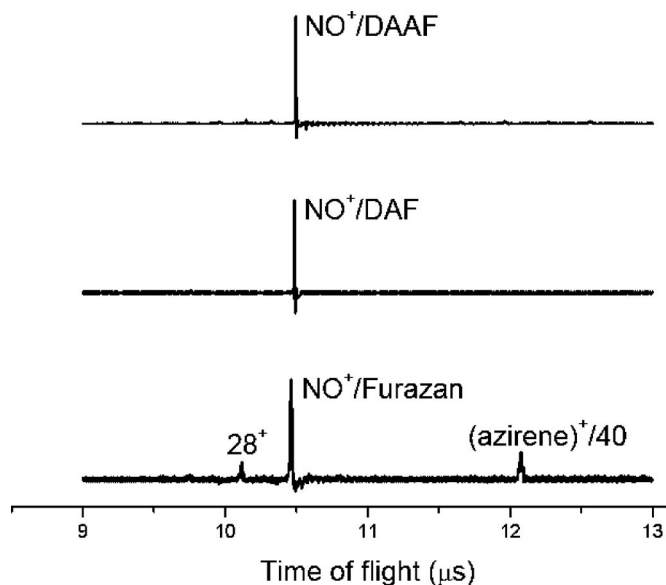


FIG. 7. Mass spectra of the excited electronic state decomposition of DAAF, DAF, and furazan using femtosecond laser pulse at 226 nm. The time duration of the femtosecond laser pulse is about 180 fs. The NO molecule is the only observed product from DAAF and DAF; two additional mass channels (28 and 40 amu) are observed from furazan.

opening mechanism with rupture of a CN and a NO bond can be proposed for the initial decomposition of furazan.

Figure 8 displays femtosecond pump-probe transients for the NO product from DAAF (b) as well as NO molecule from NO gas (a) at 226 nm. As mentioned above, the NO molecule has a resonant single photon absorption for the $A^2\Sigma^+(v'=0) \leftarrow X^2\Pi(v''=0)$ transition at 226 nm. Both pump and probe beams have the same wavelength. As described in our previous report,¹⁷ the gas phase DAAF molecule is pumped to its first excited electronic state by the pump beam, then dissociates into products which are probed by the delayed probe beam. The dynamics of the decomposition are measured via the NO molecule appearance. If decomposition

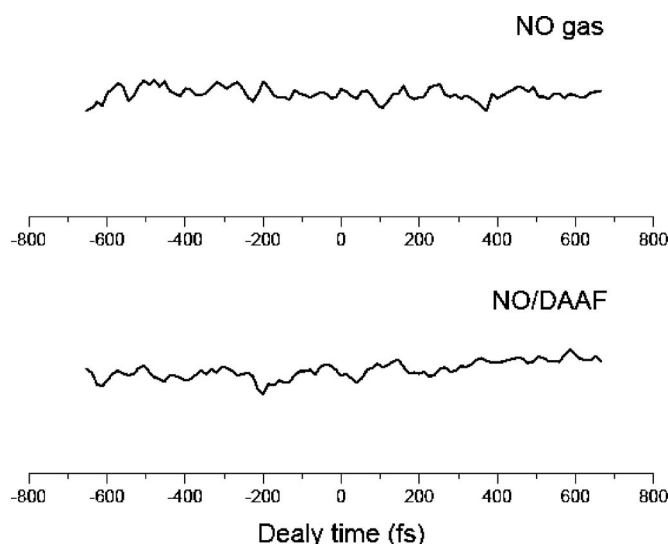


FIG. 8. One-color pump-probe transients of the NO product from NO gas and DAAF using femtosecond laser pulse at 226 nm. The NO molecule has a resonance absorption at 226 nm due to $[A^2\Sigma^+(v=0) \leftarrow X^2\Pi(v=0)]$ transition.

TABLE II. Vertical excitation energies E_{vert} and state characterization at FC geometry of furazan and DAF.

Compounds	State	E_{vert} (eV)	
		CASSCF	CAS-MP2
Furazan	$S_1/(n, \pi^*)$	6.09	4.70
	$S_2/(\pi, \pi^*)$	6.55	5.55(5.39 ^a)
DAF	$S_1/(n, \pi^*)$	6.69	4.46
	$S_2/(\pi, \pi^*)$	7.03	4.90

^aExperimental absorption maximum at 25 °C in gas phase (Ref. 28).

of DAAF is slower than the time duration of the pump and probe beams (180 fs), an (exponential) onset of the NO ion signal will be observed as the relative delay time between the pump and probe beams is scanned. If decomposition of the energetic materials is much faster than the pulse duration, NO product will be excited by the pump beam in addition to the probe beam, and the lifetime of the NO excited state, which is several hundred nanosecond, will be detected by the probe beam, and the pump-probe transient for the NO product should be a flat horizontal line within a many picosecond time interval. The transients in Fig. 8 show a roughly steady NO ion signal from DAAF, which is the same as NO gas, indicating that the decomposition dynamics of DAAF occurs on a faster time scale than the time duration of our laser pulse.

V. THEORETICAL RESULTS

In order to understand the mechanisms of the excited electronic state decomposition of furazan based energetic materials better, theoretical calculations using the CASSCF method have been performed on the two model systems, furazan and DAF.

The vertical excitation energies (E_{vert}) for furazan and DAF, calculated at their CASSCF optimized Franck-Condon (FC) geometries (ground state minimum) of C_1 symmetry are listed in Table II. The E_{vert} at the CASSCF/6-31G^{*} level of theory is calculated for comparison with relative energies of the critical points on the excited potential energy surfaces. The E_{vert} at the MP2 correlated CASSCF level of theory with the same basis set is calculated with higher accuracy for comparison with experimental excitation energies. Both CASSCF and MP2 correlated CASSCF calculations show that the two lowest-lying excited states for both furazan and DAF are (n, π^*) and (π, π^*) states, which correspond to their S_1 and S_2 excited electronic states, respectively. Moreover, the calculated vertical excitation energy of the S_2 (π, π^*) state of furazan with higher accuracy is about 5.55 eV (see Table II), which is in good agreement with the experimental value of 5.39 eV.²⁸ By comparing the three excitation energies (5.49 eV at 226 nm, 5.25 eV at 236 nm, and 5.00 eV at 248 nm) used in this work with the calculated vertical excitation energies (5.55 and 4.7 eV, Table II) of the S_2 (π, π^*) and S_1 (n, π^*) excited states of the furazan molecule, one finds that the furazan molecule is excited to its S_2 (π, π^*) excited state by these three excitation wavelengths.

TABLE III. Relative CASSCF energies (E_{rel}) of critical points, with respect to the ground state FC energies for furazan and DAF.

Compounds	Structure	E_{rel} (eV)
Furazan	$(S_2/S_0)_{\text{CI}}$	2.30
	$(S_1/S_0)_{\text{CI}}$	6.69
	TS_1/S_0	6.29
DAF	$(S_2/S_0)_{\text{CI}}$	3.05
	$(S_1/S_0)_{\text{CI}}$	6.04
	TS_1/S_0	5.60

In particular, 226 nm excitation corresponds to the absorption maximum (vertical excitation) for the S_2 (π, π^*) excited state of furazan.

The relative CASSCF energies of the critical points (minimum, conical intersections, transition state) on both excited and ground potential energy surfaces of furazan and DAF with respect to the energy of ground state FC geometry are listed in Table III. The relative energies of conical intersections $(S_2/S_0)_{\text{CI}}$ and $(S_1/S_0)_{\text{CI}}$ and transition structure TS_1/S_0 of furazan are 2.30, 6.69, and 6.29 eV, respectively. The relative energies of similar counterparts of DAF are 3.05, 6.04, and 5.6 eV, respectively. A schematic two-dimensional projection of multidimensional potential energy surfaces of furazan and DAF with locations and structures of different critical points are plotted in Figs. 9(A) and 9(B), respectively. Dotted arrows in these two figures indicate different possible decomposition channels for the excited state decomposition of furazan and DAF along different relevant nuclear coordinates. The optimized ground state geometry (FC geometry) has a planar five-membered ring for furazan and the additional amine substituents in DAF are pyramidalized (see Fig. 1). The structure of furazan at the $(S_1/S_0)_{\text{CI}}$ conical intersection [see Fig. 9(A)] is bent out of plane and is found to have similar energy to that of the absorption maximum of the spectroscopically active S_2 (π, π^*) state. The calculated transition state structure on the ground electronic surface of furazan, following the $(S_1/S_0)_{\text{CI}}$ conical intersection, shows a similar geometry to that of $(S_1/S_0)_{\text{CI}}$. The unstable vibrational mode associated with this TS is found to be a NO-azirene ($\text{C}_2\text{H}_2\text{N}$) symmetric stretch which indicates the formation of azirene along with NO elimination on the product side. This unstable vibrational mode does not generate any resultant torque acting on the NO moiety. The $(S_1/S_0)_{\text{CI}}$ conical intersection of DAF has similar structure to that of furazan [see Fig. 9(B)] and is found to be ~ 1 eV in energy lower than that of the absorption maximum for the S_2 (π, π^*) state. So the computational results suggest that due to the vertical excitation to the S_2 (π, π^*) state, a nonadiabatic dissociation pathway is possible for these two compounds from FC point of the S_2 (π, π^*) state though the $(S_1/S_0)_{\text{CI}}$ conical intersection after bypassing the $(S_2/S_1)_{\text{CI}}$ conical intersection. This suggested decomposition pathway for both molecules would generate NO products with cold rotational distributions because related transition states on their ground electronic surfaces do not generate a large resultant torque on the NO moiety.

The $(S_2/S_0)_{\text{CI}}$ for both furazan and DAF has been calcu-

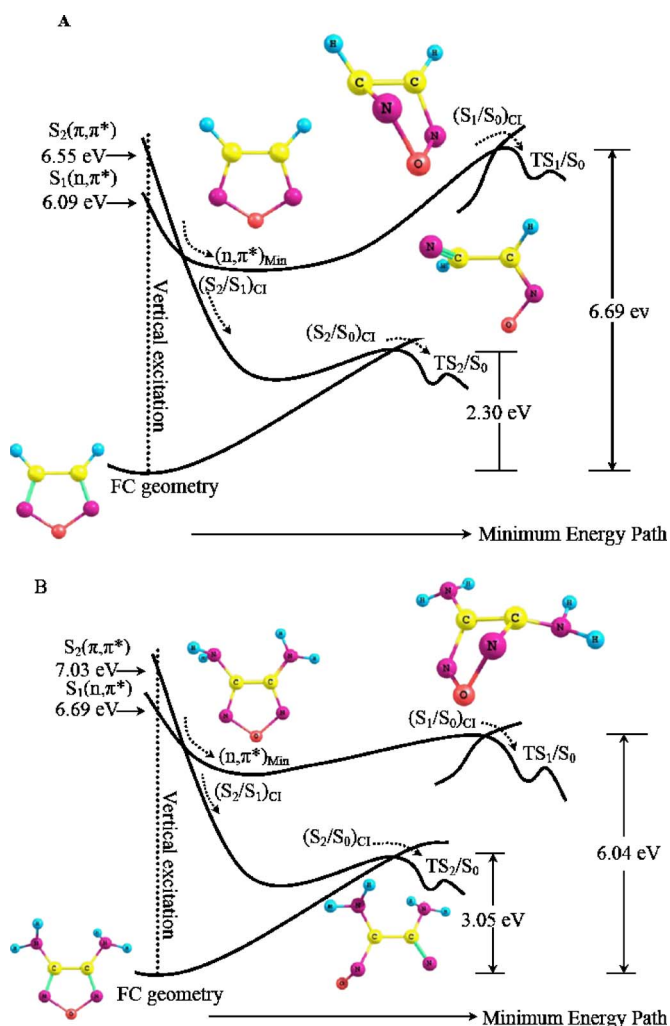


FIG. 9. (Color online) Two-dimensional projection of multidimensional potential energy surfaces of furazan (A) and DAF (B) computed at the CASSCF/6-31G* level of theory. Due to electronic excitation above the $(S_1/S_0)_{CI}$ conical intersection point, electronic energy gets thermalized by populating out-of-plane vibrationally active ring modes, which can lead the dissociation pathway along the $(S_1/S_0)_{CI}$ conical intersection followed by its decomposition to a rotationally cold NO initial product. Electronic excitation below the $(S_1/S_0)_{CI}$ conical intersection does not provide sufficient energy to surmount the $(S_1/S_0)_{CI}$ conical intersection. Under this situation, electronic energy will eventually be thermalized by repopulating another vibrationally active ring opening mode which can lead to deactivation along the $(S_2/S_0)_{CI}$ conical intersection, yielding a rotationally hot distribution for the NO product. Note that two nonadiabatic dissociation channels are along two different nuclear coordinates and CASSCF calculated energies are ~ 1 – 2 eV off from the more accurate MP2 correlated CASSCF energies. Thus the energy axis only suggests relative positions of the potential energy surfaces and intersections.

lated taking only π orbitals in the active space and has an out-of-plane open ring geometry [see Figs. 9(A) and 9(B)]. For furazan, the $(S_2/S_0)_{CI}$ conical intersection is found to be ~ 3 eV below its $(S_1/S_0)_{CI}$ conical intersection and DAF is found to have an $(S_2/S_0)_{CI}$ conical intersection ~ 4.3 eV below its $(S_1/S_0)_{CI}$ conical intersection. For both compounds, the $(S_2/S_0)_{CI}$ conical intersection is followed by a TS on their ground electronic surface (S_0). This TS has an unstable torsional mode that clearly indicates a torque acting on NO moiety for NO elimination pathway. Thereby, nonadiabatic dissociation of these two compounds from the FC point (ab-

sorption maximum) of the $S_2(\pi, \pi^*)$ state through their $(S_2/S_0)_{CI}$ conical intersection after crossing the $(S_2/S_1)_{CI}$ conical intersection can provide hot rotational distributions for the NO product.

Based on the computational results, two different nonadiabatic, radiationless dissociation pathways are possible for the decomposition mechanism of furazan and DAF from their $S_2(\pi, \pi^*)$ excited electronic state. One involves an almost barrierless nonadiabatic dissociation path from the FC point of the $S_2(\pi, \pi^*)$ state through the $(S_1/S_0)_{CI}$ conical intersection after bypassing the $(S_2/S_1)_{CI}$ conical intersection when the excitation energy is enough to surmount the $(S_1/S_0)_{CI}$ conical intersection. The other involves an alternate nonadiabatic dissociation path from the FC point of the $S_2(\pi, \pi^*)$ state through the $(S_2/S_0)_{CI}$ conical intersection after crossing the $(S_2/S_1)_{CI}$ conical intersection when the excitation energy is lower than the $(S_1/S_0)_{CI}$ conical intersection. In the first dissociation mechanism, following vertical electronic excitation to the $S_2(\pi, \pi^*)$ state, for both furazan and DAF, electronic energy can rapidly be thermalized through the $(S_1/S_0)_{CI}$ conical intersection by populating out-of-plane vibrationally active ring modes. This pathway must go via an adiabatic state switch from the spectroscopic (π, π^*) to the (n, π^*) state, bypassing the $(S_2/S_1)_{CI}$ conical intersection. This process can generate cold rotational distributions of the NO product as the unstable normal mode of vibration associated with respective transition states on their ground electronic surface do not possess any resultant torque acting on the NO moiety. In the second alternate channel, on the other hand, because electronic excitation of these molecules does not provide sufficient energy to surmount the $(S_1/S_0)_{CI}$ conical intersection, electronic energy will eventually be thermalized by populating another vibrationally active ring opening mode which can lead the deactivation along the $(S_2/S_0)_{CI}$ conical intersection, yielding a rotationally hot distribution for the NO product as the unstable normal mode of vibration associated with the related TS on the ground electronic surface has a torque acting on the NO moiety for the NO elimination pathway.

A similar computation on DAAF, the energetic material, could not be performed at the CASSCF or MP2 correlated CASSCF level of theory due to its large active space. The MP2/6-311G** optimized geometry of DAAF, shown in Fig. 1, is nonplanar.

VI. DISCUSSION

In the present work, the furazan based energetic material, DAAF, and its model systems, DAF and furazan have been studied both experimentally and theoretically to elucidate their decomposition pathways and initial fragmentation upon electronic state excitations. With regard to the furazan based energetic systems, DAAF has been our major focus thus far. We have observed only NO from any of these systems, and we conclude that it is the major initial product in their excited electronic state decomposition. NH_2 is not observed as a secondary decomposition product both in TOFMS and LIF experiments. In our experiments, each parent molecule is excited to its excited electronic state using

different excitation wavelengths (226, 236, and 248 nm) that also correspond to the resonance $A^2\Sigma^+(v'=0) \leftarrow X^2\Pi(v''=0,1,2)$ transitions of the NO molecule. The NO product from DAAF displays similar cold rotational distributions (20 K) at all three excitation wavelengths (226, 236, and 248 nm). Similar rovibronic spectral structures for the NO product from DAAF at different excitation wavelengths indicate that the excited electronic state decomposition of DAAF follows a single, excitation wavelength independent dissociation channel. The model systems, on the other hand, show excitation wavelength dependent dissociation channels. For example, dissociation of furazan at 236 nm and that of DAF at 248 nm render hot rotational distributions for the NO product, whereas excitation of furazan at 226 nm and that of DAF at 226 and 236 nm yield cold rotational distributions for the NO product. Thus, we conclude that the excited electronic state decomposition of the energetic material DAAF takes place through the same pathway at the three excitation wavelengths used in this experiment, but the excited electronic state decomposition of the model systems (DAF and furazan) takes place through two different dissociation channels depending on the excitation wavelengths.

This difference in behavior can only be rationalized by the fact that DAAF must have dissociative excited states which can provide a barrierless single deactivation channel for excited state decomposition. For the model systems, on the other hand, a barrier in the excited state decomposition pathway must exist which can alter the dissociation channel from the excited state. As an example, excitation of furazan and DAF at 226 nm (5.5 eV) can surmount an energy barrier to provide a rotationally cold (20 K) distribution for the NO product, and excitation of furazan at 236 nm (5.26 eV) and that of DAF at 248 nm (5.0 eV) do not provide sufficient energy to surmount that barrier. Eventually they follow different dissociation channels, providing hot NO rotational distributions. Moreover, the threshold excitation energies for the two different dissociation channels of the model systems must be between 5.5 eV (\sim 226 nm) and 5.25 eV (\sim 236 nm) for furazan and 5.25 eV (\sim 236 nm) and 5.0 eV (\sim 248 nm) for DAF. To get theoretical support and understanding for these experimental observations, the evolution pathways from excited electronic states with respect to the relevant reaction coordinates have to be known. We have therefore explored the potential energy surfaces for the model systems furazan and DAF, shown in Figs. 9(A) and 9(B). Note that two nonadiabatic dissociation channels are along two different nuclear co-ordinates and CASSCF calculated energies are \sim 1–2 eV off from the MP2 correlated CASSCF energies.

Conical intersections are now firmly established to be the key features in the excited electronic state chemistry of the polyatomic molecules.^{29–31} The concept of a conical intersection was first introduced by von Neumann and Wigner³² and has been now recognized as essential for describing the dynamics and mechanisms for deactivation of a vast range of polyatomic molecules from their excited electronic states to their ground electronic surface.^{33–37} One of their most important implications is the rapid and efficient internal conversion from upper to lower electronic state sur-

faces through radiationless transitions. A radiationless transition through a conical intersection involves rapid conversion of electronic energy belonging to the upper electronic state to vibrational energies (thermal energies) of the lower electronic state. As mentioned in Sec. V, the excitation wavelengths used in our experiment correspond to the transition to the $S_2(\pi, \pi^*)$ excited state of the furazan heteroaromatic rings, and, in particular, 226 nm excitation corresponds to the absorption maximum (vertical excitation) for the $S_2(\pi, \pi^*)$ excited state of furazan. Thus, for furazan, the existence of the $(S_1/S_0)_{CI}$ conical intersection [see Fig. 9(A)] at almost the same energy as that of the absorption maximum of the spectroscopically active $S_2(\pi, \pi^*)$ state indicates that due to excitation to the $S_2(\pi, \pi^*)$ state at 226 nm, electronic energy can be rapidly thermalized through an almost barrierless nonadiabatic dissociation pathway from the FC point (absorption maximum) of the $S_2(\pi, \pi^*)$ state through the $(S_1/S_0)_{CI}$ conical intersection by populating out-of-plane vibrationally active ring mode. This dynamical process will generate NO product with cold rotational distributions, as the unstable normal mode of vibration associated with the relevant transition state on the ground electronic state surface do not generate a resultant torque on the NO moiety during dissociation of the parent molecule. In this dynamical process, the adiabatic state switch from the spectroscopic (π, π^*) to the (n, π^*) state must occur by bypassing the $(S_2/S_1)_{CI}$ conical intersection.

At 236 nm excitation, on the other hand, furazan cannot surmount the energy barrier for the $(S_1/S_0)_{CI}$ conical intersection since 236 nm excitation energy is about 0.25 eV lower than that of 226 nm. Rather this electronic energy eventually gets thermalized by the repopulation of other vibrationally active ring opening modes through intramolecular vibrational energy redistribution (IVR); these modes can follow another nonadiabatic dissociation channel through the $(S_2/S_0)_{CI}$ conical intersection after crossing the $(S_2/S_1)_{CI}$ conical intersection. This decomposition pathway can result in a rotationally hot distribution of NO, as the relevant TS on the ground electronic state surface following the $(S_2/S_0)_{CI}$ conical intersection is associated with an unstable torsional degree of freedom, which generates a torque on the NO moiety during dissociation of the parent molecule. Thus, the proposed mechanism suggests that excited electronic state decomposition of furazan at 226 and 236 nm excitations involves two different nonadiabatic dissociation pathways yielding NO as the initial decomposition product. The NO product due to the excited electronic state decomposition of furazan at 226 nm excitation is rotationally cold and that at 236 nm excitation is rotationally hot, in good agreement with experimental observations.

In addition, we conclude that, when the molecule has high enough energy to surmount the energy barrier for the $(S_1/S_0)_{CI}$ conical intersection, it undergoes nonadiabatic dissociation predominately following the $(S_1/S_0)_{CI}$ conical intersection not through the $(S_2/S_1)_{CI}$ conical intersection. One reason for this conclusion is that if 226 nm excitation can access both nonadiabatic decay channels through $(S_1/S_0)_{CI}$ and $(S_2/S_1)_{CI}$ conical intersections with equal probabilities, then one should observe hot rovibronic structure for NO

from 226 nm excitation of furazan convoluted with cold rovibronic structures in the nanosecond laser experiments. Instead, we observe only a cold rotational distribution of NO from decomposition of furazan at 226 nm excitation. If the molecule, on the other hand, does not have sufficient energy to surmount the energy barrier for the $(S_1/S_0)_{CI}$ conical intersection, it will eventually follow the other nonadiabatic decay channel crossing the $(S_2/S_1)_{CI}$ conical intersection followed by internal conversion to the ground state through the $(S_2/S_0)_{CI}$ conical intersection rendering hot rotational distribution for the NO product. Wavepacket dynamics calculations and femtosecond pump-probe experiments for furazan are needed to confirm the influence of the limiting factors, adiabatic state switching and IVR on the proposed decomposition dynamics of furazan from its excited electronic state.

A similar $(S_1/S_0)_{CI}$ conical intersection [shown in Fig. 9(B)] for DAF is found ~ 1 eV in energy below its vertical excitation energy. Thus, excitation of DAF at both 226 and 236 nm can follow the nonadiabatic dissociation pathway through the $(S_1/S_0)_{CI}$ conical intersection, but the 248 nm excitation of DAF cannot surmount that energy barrier. Rather DAF dissociates following 248 nm excitation along the $(S_2/S_0)_{CI}$ conical intersection resulting in a rotationally hot distribution of NO. Thus the proposed mechanism suggests that the excited electronic state decomposition of DAF at 226 and 236 nm excitations involves a single nonadiabatic dissociation pathway yielding only rotationally cold distribution of the NO product. At 248 nm excitation of DAF, another nonadiabatic dissociation pathway is opened rendering a rotationally hot distribution of NO. This mechanism is in good agreement with experimental observations.

As DAAF has generated only rotationally cold distributions of the NO product due to excitation at three different excitation energies, we extrapolate that the excited electronic states of DAAF are dissociative in nature and that the DAAF conical intersection between the (n, π^*) excited state and ground electronic state, $(n, \pi^*/gs)_{CI}$ [similar to the $(S_1/S_0)_{CI}$ for DAF and furazan] is even lower in energy than that for DAF. Thus the suggested DAAF $(n, \pi^*/gs)_{CI}$ conical intersection can be readily accessible by electronic excitations at all of the three excitation wavelengths used in our experiment. This energetically accessible $(n, \pi^*/gs)_{CI}$ conical intersection can provide DAAF a very efficient, unique, and single pathway to release its entire chemical energy from random electronic excitations to its (π, π^*) excited electronic state during the detonation of this energetic material simply initiated by compression or shockwaves. The model systems, on the other hand, suffer from not having an efficient single pathway to release their entire chemical energy during excited electronic state decompositions of these species. One pathway for the model systems provides rotationally cold NO product and another provides rotationally hot NO product. Thereby, the energy barrier for the $(n, \pi^*/gs)_{CI}$ conical intersection with respect to excitation wavelengths plays a crucial role in the decomposition mechanism of these molecules, and thus DAAF, being an energetic material, behaves differently from its nonenergetic model systems. The pump-probe transient for the NO product at resonant wave-

length indicates that the decomposition dynamics of DAAF falls within the time scale of our femtosecond laser pulse duration (180 fs).

VII. CONCLUSIONS

The excited electronic state decomposition of DAAF and those of its model systems have been investigated via nanosecond energy resolved and femtosecond time resolved spectroscopies. Both DAAF and its model systems generate NO as an initial decomposition product; however, at the nanosecond laser excitation wavelengths, vibrational and rotational distributions of the NO product are quite different. DAAF generates the NO product with only cold rotational (20 K) and hot vibrational (1260 K) distributions that are independent of excitation wavelengths. On the contrary, the model systems generate different rotational distributions for NO depending on the excitation wavelengths employed for the excited electronic state decomposition of the parent molecules. Based on the experimental observations and CASSCF calculations, we conclude that the excited electronic state decomposition of DAAF occurs through a unique, single, nonadiabatic dissociation channel that is independent of excitation wavelengths. The model systems (DAF and furazan) dissociate through two different nonadiabatic dissociation channels, which depend on excitation wavelengths. In this case, the energy barrier for the $(S_1/S_0)_{CI}$ conical intersection with respect to excitation energy plays a crucial role in the initial excited electronic state decomposition of the model systems. Based on these results, a five-membered heterocyclic furazan ring opening mechanism is suggested with rupture of CN and NO bonds yielding NO as the major decomposition product. The dynamics of NO generated from DAAF is found to fall within the time scale of our laser pulse duration (180 fs). NH_2 is not observed as a secondary decomposition product of either DAAF or DAF.

ACKNOWLEDGMENTS

These studies are supported by grants from ARO and the DOD DURIP program. We are grateful to Mike Hiskey and Daren Naud (LANL) for giving us DAAF and other energetic materials.

- ¹M. A. Hiskey, D. E. Chavez, R. L. Bishop, J. F. Kramer, and S. A. Kinkead, U.S. Patent No. 6,358,339 (19 March 2002).
- ²D. E. Chavez, M. A. Hiskey, and R. D. Gilardi, *Angew. Chem., Int. Ed.* **39**, 1791 (2000).
- ³D. E. Chavez, L. Hill, M. Hiskey, and S. Kinkead, *J. Energ. Mater.* **18**, 219 (2000).
- ⁴D. E. Chavez and M. A. Hiskey, *Journal of Pyrotechnics* **7**, 11 (1998).
- ⁵M. B. Talawar, R. Sivabalan, N. Senthikumar, G. Prabhu, and S. N. Asthana, *J. Hazard. Mater.* **113**, 11 (2004).
- ⁶M. B. Talawar, J. K. Nair, S. M. Pundalik, R. S. Satpute, and S. Venugopalan, *J. Hazard. Mater.* **136**, 978 (2006).
- ⁷T. S. Cantrell and W. S. Haller, *Chem. Commun. (Cambridge)* **1968**, 977.
- ⁸V. G. Prokudin and G. M. Nazin, *Bull. Acad. Sci. USSR Div. Chem. Sci. (Engl. Transl.)* **36**, 199 (1987).
- ⁹F. J. Owens and J. Sharma, *J. Appl. Phys.* **51**, 1494 (1979).
- ¹⁰J. Sharma and B. C. Beard, in *Structures and Properties of Energetic Materials*, MRS symposia Proceedings No. 296, edited by D. H. Liedenbergh, R. W. Armstrong, and J. J. Gilman (Materials Research Society, Pittsburgh, Pennsylvania, 1993).
- ¹¹J. J. Gilman, *Philos. Mag. B* **589**, 379 (1992).

- ¹²B. P. Aduiev, E. D. Aluker, G. M. Belokurov, and A. G. Krechetov, *Chem. Phys. Rep.* **16**, 1479 (1997).
- ¹³A. B. Kunz, M. M. Kuklja, T. R. Botcher, and T. P. Russell, *Thermochim. Acta* **384**, 279 (2002).
- ¹⁴E. R. Bernstein, in *Overviews of Recent Research on Energetic Materials*, edited by D. Thompson, T. Brill, and R. Shaw (World Scientific, Hackensack, NJ, 2004).
- ¹⁵H.-S. Im and E. R. Bernstein, *J. Chem. Phys.* **113**, 7911 (2000).
- ¹⁶Y. Q. Guo, M. Greenfield, and E. R. Bernstein, *J. Chem. Phys.* **122**, 244310 (2005).
- ¹⁷M. Greenfield, Y. Q. Guo, and E. R. Bernstein, *Chem. Phys. Lett.* **430**, 277 (2006).
- ¹⁸Y. Q. Guo, M. Greenfield, A. Bhattacharya, and E. R. Bernstein, *J. Chem. Phys.* **127**, 154301 (2007).
- ¹⁹R. Trebino, *Frequency-Resolved Optical Grating: The Measurement of Ultrafast Laser Pulses* (Kluwer Academic, Boston, 2000).
- ²⁰M. Foltin, G. J. Stueber, and E. R. Bernstein, *J. Chem. Phys.* **114**, 8971 (2001).
- ²¹M. Foltin, G. J. Stueber, and E. R. Bernstein, *J. Chem. Phys.* **111**, 9577 (1999).
- ²²P. Carcabal, R. T. Kroemer, L. C. Snoek, J. P. Simons, J. M. Bakker, I. Compagnon, G. Meijer, and G. von Helden, *Phys. Chem. Chem. Phys.* **6**, 4546 (2004).
- ²³L. C. Snoek, T. van Mourik, and J. P. Simons, *Mol. Phys.* **101**, 1239 (2003).
- ²⁴M. J. Frisch, G. W. Trucks, H. B. Schlegel *et al.*, GAUSSIAN 03, Gaussian Inc., Pittsburgh, PA, 2003.
- ²⁵M. Hippler and J. Pfab, *Chem. Phys. Lett.* **243**, 500 (1995).
- ²⁶G. Herzberg, *Spectra of Diatomic Molecules* (Van Nostrand, New York, 1950), p. 257.
- ²⁷Y. G. Byun, S. Saebo, and C. U. Pittman, *J. Am. Chem. Soc.* **113**, 3689 (1991).
- ²⁸B. J. Forrest and A. W. Richardson, *Can. J. Chem.* **50**, 2088 (1972).
- ²⁹W. Domcke, D. R. Yarkony, and H. Koppel, *Conical Intersections: Electronic Structure, Dynamics and Spectroscopy* (World Scientific, River Edge, NJ, 2003).
- ³⁰G. A. Worth and L. S. Cederbaum, *Annu. Rev. Phys. Chem.* **55**, 127 (2004).
- ³¹*The Role of Degenerate States in Chemistry*, Advances in Chemical Physics Vol. 124, edited by M. Baer and G. D. Billing (J. Wiley and Sons, Hoboken, NJ, 2002), p. 124.
- ³²J. von Neumann and E. Wigner, *Z. Phys.* **30**, 467 (1929).
- ³³J. Soto, J. F. Arenas, J. C. Otero, and D. Pelaez, *J. Phys. Chem. A* **110**, 8221 (2006).
- ³⁴L. Serrano-Andres, M. Merchan, and A. C. Borin, *Proc. Natl. Acad. Sci. U.S.A.* **103**, 8691 (2006).
- ³⁵N. Ismail, L. Blancafort, M. Olivucci, B. Kohler, and M. A. Robb, *J. Am. Chem. Soc.* **124**, 6818 (2002).
- ³⁶L. Blancafort, *J. Am. Chem. Soc.* **128**, 210 (2006).
- ³⁷C. Canuel, M. Elhanine, M. Mons, F. Piuze, B. Tardivel, and I. Dimicoli, *Phys. Chem. Chem. Phys.* **8**, 3978 (2006).